

PACS numbers: 42.50.Gy; 42.79.Vb
DOI: 10.1070/QE2011v041n12ABEH014466

All-optical loadable and erasable memory cell design based on inversionless lasing and electromagnetically induced transparency effects

N. Gholipour Verki, A. Hajibadali, K. Abbasian, A. Rostami

Abstract. **A loadable and erasable all-optical memory cell is designed by using two coupled micro-ring resonators with electromagnetically induced transparency (EIT) and lasing without inversion (LWI). To read out stored data, an additional phase is introduced in the upper ring resonator due to EIT. To compensate the fibre loss, use is made of LWI. The EIT is induced by inserting Λ-type three level quantum dots in the right-hand half of the upper ring and LWI is implemented by inserted Y-type four level quantum dots in the left-hand half of both rings. This optical memory cell can operate at a low light power level corresponding to several photons.**

Keywords: *micro-ring resonator, memory cell, quantum dot, lasing without inversion, electromagnetically induced transparency.*

1. Introduction

There is an increasing demand in high-throughput networks supporting data transmission rates on the order of several hundred terabits per second for voice, video, image, and data applications. Thus, an all-optical memory is one of the important elements for quantum and classical optical information processing and communication. To design an all-optical memory, different approaches are examined. Nevertheless, the problem still remains unsolved. Highly integrated photonic circuits are required for future compact communication systems [1]. Due to their wavelength-scale dimensions and high quality factors, a micro-ring resonator is a promising device which can be widely used as basic building block of such integrated photonic systems. Besides, micro-ring resonators are used in various optical components, e.g., optical filters [2–4], switches, modulators [5, 6], sensors [7] and optical memories [8].

Advances in the field of all-optical techniques for information processing include improvement of buffers [9], registers, etc. The memory cell is one of the key building blocks that can be used to implement a variety of all-optical processing applications, including optical packet storage. Several types of serial optical memory suitable for storing optical packets have been demonstrated using recirculating optical fibre loops [10].

N. Gholipour Verki Technical & Engineering Faculty of Bonab, University of Tabriz, Tabriz 51666, Iran;
A. Hajibadali Electrical and Computer Department, Sabzevar Tarbiat Moallem University, Sabzevar, Iran;
K. Abbasian, A. Rostami School of Engineering-Emerging Technologies, University of Tabriz, Tabriz 51666, Iran;
e-mail: K_abbasian@tabrizu.ac.ir

Received 15 October 2011
Kvantovaya Elektronika **41** (12) 1114–1118 (2011)
Submitted in English

A promising optical memory was demonstrated by dual micro-ring lasers using an injection lock. However, this method is not convenient for serial connection because counterpropagating clockwise and counterclockwise directions are the directions of the two operating laser modes. The flip-flop memory is one of the most interesting memory types. However, realisation of ultrafast flip-flop operation with the picosecond switch time for the GHz data memory is still a great challenge [11]. Therefore, Yunhong Ding et al. [12] demonstrated a loadable and erasable optical memory cell based on an active micro-ring optical integrator associated with III–V electroabsorption modulators (EAMs). Another promising approach was proposed for designing a loadable and erasable optical memory cell based on dual micro-ring optical integrators. The optical integrator, which can generate an optical step function for data storing, is synthesised using active media for loss compensation and a tunable phase shifter for data reading at any time. The phase shifter can be realised by cross phase-modulation induced by another control light [as in a semiconductor optical amplifier (SOA)] or by changing the carrier density induced by an electro-optic (EO) effect using laterally integrated p–i–n diodes. The gain medium can be implemented using active waveguides made of InGaAsP/InP materials or using a porous silicon waveguide (doped with Er^{3+} and Yb^{3+}) on a dielectric insulator, pumped by a 980-nm laser [11].

In this paper, we have simulated a loadable and erasable optical memory cell based on dual micro-ring optical integrators coupled via a 3×3 coupler with EIT and LWI. These dual optical integrators can realise a scheme of a controllable optical memory cell with a phase shift element introduced to read stored data and with an active medium for loss compensation. The phase shifter and required gain is realised by electromagnetically induced transparency and lasing without inversion, respectively.

The main reason for selecting such a structure is the development of an all-optical memory cell. As far as we know, this can be done at the present level of technology by using the EIT and LWI effects. On the other hand, any information has advantages and disadvantages. In our opinion, the complexity of the considered all-optical systems is an admissible disadvantage, at least till now advantages of all-optical systems have outweighed their disadvantages.

2. Theory and mathematical background

The scheme of the all-optical memory cell, based on the concept of an optical integrator with one micro-ring [13], is presented in Fig. 1. The scheme contains two micro-rings with gain media as optical integrators of the same size, coupled via a 3×3 coupler. The upper integrator has a phase shifter, which

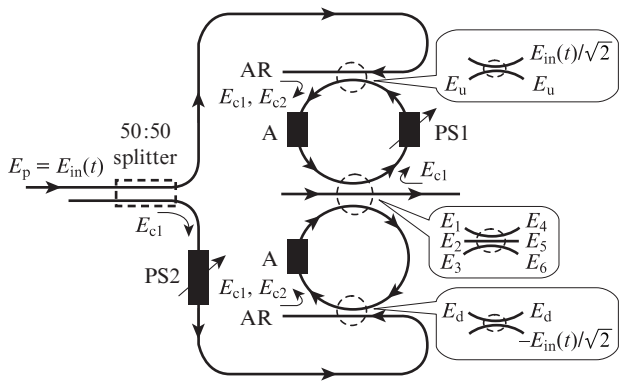

Figure 1. Scheme of the all-optical memory cell [11]: (AR) antireflection coating; (A) amplifier (due to LWI); (PS1) phase shifter $\Delta\phi_{max} = \pi$ (due to EIT); (PS2) phase shifter $\Delta\phi = \pi/2$ (due to EIT).

plays a critical role for the data reading process. In Fig. 1 $E_{in}(t)$ is the field of injected data pulse from the input port, which is split into two beams by a lossless and polarisation independent 50:50 splitter. The light field injected into the upper integrator is equal to $E_{in}(t)/\sqrt{2}$. The stored light field in the upper integrator is denoted by $E_4(t)$. An additional phase shift $\pi/2$ is introduced into the field of the lower light beam so that the light field injected into the lower integrator is equal to $-E_{in}(t)/\sqrt{2}$. The output field from the memory cell is denoted by $E_5(t)$. If the stable light field amplitude in the upper integrator can be described by $E_1 = E_{int}$, the stable light field amplitude in the lower integrator will be $E_3 = -E_{int}$. In the upper integrator the light field phase changes by $\Delta\phi(t)$. The phase shifter can be realised by cross phase-modulation induced by electromagnetically induced transparency and the gain medium is implemented by lasing without inversion in media containing Λ-type three level quantum dots and Y-type four level quantum dots, respectively. The light field in the integrator is described by [11]

$$\tilde{E}_j = E_j \exp(i\phi) \quad (j = u, d), \tag{1}$$

where u and d represent fields in the upper and lower integrators, respectively; E_j is the light field amplitude; $\phi = k_{eff} z$ is the light field phase; and z is the propagation direction. Then, the amplitude and phase propagation equation can be written in the form [11]

$$\frac{\partial E_j}{\partial Z} = (g - \alpha) E_j, \quad \frac{\partial \phi}{\partial Z} = k_{eff}, \tag{2}$$

where g and α are the gain and loss coefficients. In the right-hand half of the upper integrator, we used three-level quantum dots to implement the phase shifter. Therefore, the equation for the light field phase in the upper ring has the form

$$\phi_{ph-sh} = \phi(z = z_p) + \Delta\phi(t), \tag{3}$$

where z_p is an optional position of the phase shifter in the right-hand side of the ring. The light field in the 2×2 coupler is given by

$$E_j' = \sqrt{1 - \alpha'} E_j - i\sqrt{\alpha'} E_{in}^j \quad (j = u, d), \tag{4}$$

where E_{in}^j is the optical data bit injected into the optical integrator, $E_{in}^u = -E_{in}^d = E_{in}/\sqrt{2}$ is the input field at the input port of the memory cell.

The length of two integrators should be equal; otherwise, there will be a phase shift between the fields of these integrators. Therefore, the upper and lower integrators would be identical with the same gain g, loss α, loop delay τ, length L and have a polarisation independent 2×2 coupler. However, we have a phase shifter in the upper integrator. The 3×3 coupler between the upper and lower integrators is symmetrical; the coupler is also assumed to be lossless and polarisation independent, and its transmission characteristics can be described by the matrix [11]:

$$T = \begin{bmatrix} \frac{1}{2}(1 + \cos(\sqrt{2}\eta)) & i\frac{\sqrt{2}}{2}\sin(\sqrt{2}\eta) & -\frac{1}{2}(1 - \cos(\sqrt{2}\eta)) \\ i\frac{\sqrt{2}}{2}\sin(\sqrt{2}\eta) & \cos(\sqrt{2}\eta) & i\frac{\sqrt{2}}{2}\sin(\sqrt{2}\eta) \\ -\frac{1}{2}(1 - \cos(\sqrt{2}\eta)) & i\frac{\sqrt{2}}{2}\sin(\sqrt{2}\eta) & \frac{1}{2}(1 + \cos(\sqrt{2}\eta)) \end{bmatrix}, \tag{5}$$

where $\eta = \sqrt{2}\pi/4$ characterises the coupling strength between two adjacent waveguides of the 3×3 coupler. Also, the light fields in the 3×3 coupler satisfy the equation

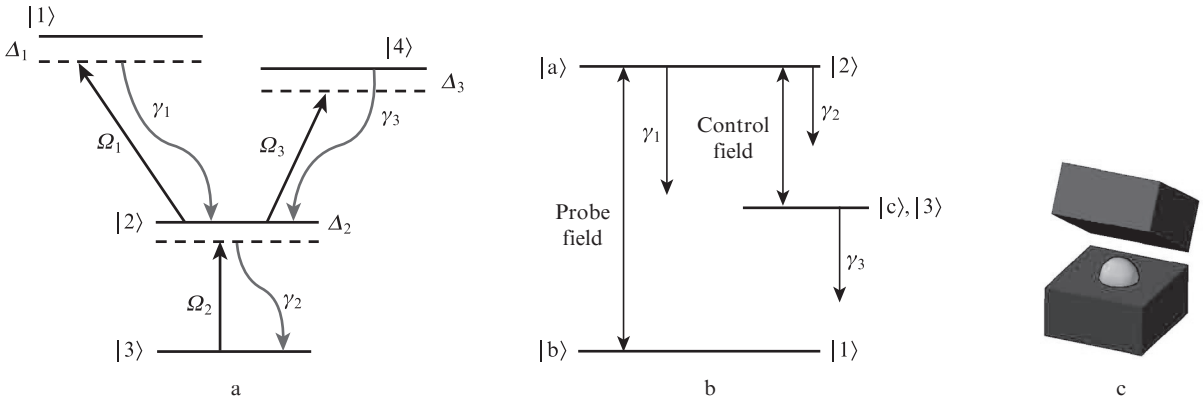

Figure 2. (a) Scheme of a Y-type four level quantum dot, (b) a Λ-type three level quantum dot and (c) three-dimensional representation of a quantum dot.

$$\begin{bmatrix} E_4 \\ E_5 \\ E_6 \end{bmatrix} = T \begin{bmatrix} E_1 \\ E_2 \\ E_3 \end{bmatrix} = \begin{bmatrix} \frac{1}{2}(E_1 - E_3) \\ \mathrm{i}\frac{\sqrt{2}}{2}(E_1 + E_3) \\ -\frac{1}{2}(E_1 - E_3) \end{bmatrix}. \quad (6)$$

We have obtained the required gain due to LWI, which is implemented by inserting Y-type four level quantum dots in the left-hand half of both rings (Fig. 2a).

In Fig. 2a, $\gamma_1, \gamma_2, \gamma_3$ correspond to spontaneous decay rates of atomic system levels. The control laser field with the Rabi frequency $\Omega_3 = d_{42}E_3/\hbar$ is nearly resonant with the transition $|2\rangle \leftrightarrow |4\rangle$. The control laser field with the Rabi frequency $\Omega_2 = d_{23}E_3/\hbar$ is nearly resonant with the transition $|3\rangle \leftrightarrow |2\rangle$, and the probe laser field with the Rabi frequency $\Omega_1 = d_{12}E_2/\hbar$ is nearly resonant with the transition $|2\rangle \leftrightarrow |1\rangle$ (here d_{12}, d_{23}, and d_{42} are the dipole matrix elements of the corresponding transitions). The quantities $\Delta_1 = \omega_{12} - \nu_1$, $\Delta_2 = \omega_{23} - \nu_2$ and $\Delta_3 = \omega_{42} - \nu_3$ represent the corresponding detunings of frequencies $\nu_{1,2,3}$ [14].

Equations for the wave functions and for the total Hamiltonian are given by

$$|\psi(t)\rangle = c_1(t)\exp(-\mathrm{i}\omega_1 t)|1\rangle + c_2(t)\exp(-\mathrm{i}\omega_2 t)|2\rangle + c_3(t)\exp(-\mathrm{i}\omega_3 t)|3\rangle + c_4(t)\exp(-\mathrm{i}\omega_4 t)|4\rangle, \quad (7)$$

$$H = H_0 + H_1, \quad (8)$$

where

$$H_0 = \hbar[\omega_1|1\rangle\langle 1| + \omega_2|2\rangle\langle 2| + \omega_3|3\rangle\langle 3| + \omega_4|4\rangle\langle 4|], \quad (9)$$

$$H_1 = -\frac{\hbar}{2}[\Omega_1\exp(-\mathrm{i}\phi_1 t)\exp(-\mathrm{i}\nu_1 t)|1\rangle\langle 2| + \Omega_2\exp(-\mathrm{i}\phi_2 t)\exp(-\mathrm{i}\nu_2 t)|2\rangle\langle 3| + \Omega_3\exp(-\mathrm{i}\phi_3 t)\exp(-\mathrm{i}\nu_3 t)|4\rangle\langle 2|] + \text{H.c.} \quad (10)$$

We consider dipole allowed atomic transitions $|2\rangle \leftrightarrow |1\rangle$, $|2\rangle \leftrightarrow |4\rangle$ and $|3\rangle \leftrightarrow |2\rangle$. We assume that the population is initially in the ground level $|3\rangle$:

$$\rho_{11}^{(0)} = \rho_{22}^{(0)} = \rho_{44}^{(0)} = 0, \quad \rho_{33}^{(0)} = 1. \quad (11)$$

The equations of motion for the density matrix elements have the form

$$\dot{\rho} = -\frac{\mathrm{i}}{\hbar}[H,\rho] = -\frac{\mathrm{i}}{\hbar}(H\rho - \rho H), \quad (12)$$

$$\begin{aligned}
\dot{\rho}_{12} &= -(\gamma_1 + \gamma_2 + \mathrm{i}\Delta_1)\rho_{12} - (\tfrac{\mathrm{i}}{2}\Omega_3\exp(\mathrm{i}\phi_3))\rho_{14} - (\tfrac{\mathrm{i}}{2}\Omega_2\exp(\mathrm{i}\phi_2))\rho_{13} - \eta\rho_{24},\\
\dot{\rho}_{14} &= -(\tfrac{\mathrm{i}}{2}\Omega_3\exp(\mathrm{i}\phi_3))\rho_{12} - (\gamma_1 + \gamma_3 + \mathrm{i}(\Delta_1 - \Delta_3))\rho_{14} + (\tfrac{\mathrm{i}}{2}\Omega_1\exp(\mathrm{i}\phi_1))\rho_{24},\\
\dot{\rho}_{23} &= -(\gamma_2 + \mathrm{i}\Delta_2)\rho_{23} + (\tfrac{\mathrm{i}}{2}\Omega_3\exp(\mathrm{i}\phi_3))\rho_{34} + (\tfrac{\mathrm{i}}{2}\Omega_1\exp(\mathrm{i}\phi_1))\rho_{13} + \tfrac{\mathrm{i}}{2}\Omega_2\exp(\mathrm{i}\phi_2),\\
\dot{\rho}_{34} &= -(\tfrac{\mathrm{i}}{2}\Omega_3\exp(\mathrm{i}\phi_3))\rho_{23} - (\gamma_3 - \mathrm{i}(\Delta_2 + \Delta_3))\rho_{34} - \eta\rho_{13} + (\tfrac{\mathrm{i}}{2}\Omega_2\exp(\mathrm{i}\phi_2))\rho_{24},\\
\dot{\rho}_{13} &= -(\tfrac{\mathrm{i}}{2}\Omega_2\exp(\mathrm{i}\phi_2))\rho_{12} + (\tfrac{\mathrm{i}}{2}\Omega_1\exp(\mathrm{i}\phi_1))\rho_{23} - \eta\rho_{34} - (\gamma_1 + \mathrm{i}(\Delta_1 + \Delta_2))\rho_{13},\\
\dot{\rho}_{24} &= -\eta\rho_{12} + (\tfrac{\mathrm{i}}{2}\Omega_1\exp(\mathrm{i}\phi_1))\rho_{14} + (\tfrac{\mathrm{i}}{2}\Omega_2\exp(-\mathrm{i}\phi_2))\rho_{34} - (\gamma_2 + \gamma_3 - \mathrm{i}\Delta_3)\rho_{24}.
\end{aligned} \quad (13)$$

The terms with $\eta = p\sqrt{\gamma_1\gamma_3}$ in equation (13) represent the vacuum-induced coherence, the parameter p is defined as $p = d_{12}d_{42}/(|d_{12}||d_{42}|) = \cos\phi$, where ϕ is the angle between the dipole matrix elements d_{12} and d_{42}.

This system of equations can be written in the matrix form

$$\dot{R} = -MR + A, \quad (14)$$

$$\dot{R} = \begin{bmatrix} \dot{\rho}_{12} \\ \dot{\rho}_{14} \\ \dot{\rho}_{23} \\ \dot{\rho}_{34} \\ \dot{\rho}_{13} \\ \dot{\rho}_{24} \end{bmatrix}, \quad R = \begin{bmatrix} \rho_{12} \\ \rho_{14} \\ \rho_{23} \\ \rho_{34} \\ \rho_{13} \\ \rho_{24} \end{bmatrix}, \quad A = \begin{bmatrix} 0 \\ 0 \\ \frac{\mathrm{i}}{2}\Omega_2\exp(-\mathrm{i}\phi_2) \\ 0 \\ 0 \\ 0 \end{bmatrix}, \quad (15)$$

$$M = \begin{bmatrix}
\gamma_1 + \gamma_2 + \mathrm{i}\Delta_1 & \frac{\mathrm{i}}{2}\Omega_3\exp(\mathrm{i}\phi_3) & 0 & 0 & \frac{\mathrm{i}}{2}\Omega_2\exp(\mathrm{i}\phi_2) & p\sqrt{\gamma_1\gamma_3} \\
\frac{\mathrm{i}}{2}\Omega_3\exp(\mathrm{i}\phi_3) & \gamma_1 + \gamma_3 + \mathrm{i}(\Delta_1 - \Delta_3) & 0 & 0 & 0 & -\frac{\mathrm{i}}{2}\Omega_1\exp(-\mathrm{i}\phi_1) \\
0 & 0 & \gamma_2 + \mathrm{i}\Delta_2 & -\frac{\mathrm{i}}{2}\Omega_3\exp(-\mathrm{i}\phi_3) & -\frac{\mathrm{i}}{2}\Omega_1\exp(\mathrm{i}\phi_1) & 0 \\
0 & 0 & \frac{\mathrm{i}}{2}\Omega_3\exp(-\mathrm{i}\phi_3) & \gamma_3 - \mathrm{i}(\Delta_2 + \Delta_3) & p\sqrt{\gamma_1\gamma_3} & -\frac{\mathrm{i}}{2}\Omega_2\exp(\mathrm{i}\phi_2) \\
\frac{\mathrm{i}}{2}\Omega_2\exp(\mathrm{i}\phi_2) & 0 & -\frac{\mathrm{i}}{2}\Omega_1\exp(-\mathrm{i}\phi_1) & p\sqrt{\gamma_1\gamma_3} & \gamma_1 - \mathrm{i}(\Delta_1 + \Delta_2) & 0 \\
p\sqrt{\gamma_1\gamma_3} & -\frac{\mathrm{i}}{2}\Omega_1\exp(\mathrm{i}\phi_1) & 0 & -\frac{\mathrm{i}}{2}\Omega_2\exp(\mathrm{i}\phi_2) & 0 & \gamma_2 + \gamma_3 - \mathrm{i}\Delta_3
\end{bmatrix}. \quad (16)$$

By solving the above equations, we obtain

$$\rho_{12} = R(1,1) = \sum_{j=1}^{6} M^{-1}(1,j)\,A(j,1)$$

$$= M^{-1}(1,3)\,A(3,1). \qquad (17)$$

By using the macroscopic polarisation equation, the equation for the susceptibility can be written in the form

$$\chi = \frac{P}{\varepsilon_0 E} = \frac{2N_a \wp^2 \rho_{ab}}{\varepsilon_0 \Omega_1 \hbar}, \qquad (18)$$

where Ω_1 is the Rabi frequency of the probe field, $\wp$ are the dipole matrix elements and N_a is the atom number density;

$$\chi = \chi' + i\chi'', \qquad (19)$$

where χ' и χ'' are the real and imaginary parts of the complex susceptibility.

Thus, the gain is

$$g = -\frac{k}{2}\chi''. \qquad (20)$$

The phase shifter in the upper integrator is implemented by EIT, which is induced by the Λ-type three level quantum dots inserted in the right-hand half of the upper ring, as shown in Fig. 2b.

After some similar mathematical manipulations, the real and imaginary parts of the optical susceptibility for the Λ-type three level quantum dot are given by

$$\chi' = -\frac{N_a \wp_{ab}^2}{\varepsilon_0 \hbar Z}[\gamma_3(\gamma_1+\gamma_3) + (\Delta^2 - \gamma_1\gamma_3 - \Omega_\mu^2/4)], \qquad (21)$$

$$\chi'' = -\frac{N_a \wp_{ab}^2}{\varepsilon_0 \hbar Z}[\Delta^2(\gamma_1+\gamma_3) - \gamma_3(\Delta^2 - \gamma_1\gamma_3 - \Omega_\mu^2/4)], \qquad (22)$$

where $Z = (\Delta^2 - \gamma_1\gamma_2 - \Omega_\mu^2/4)^2 + \Delta^2(\gamma_1+\gamma_2)^2$, $\Delta = \omega_{ab} - \nu$, γ_1, γ_2, γ_3, Ω_μ and N_a are the detunings of the probe frequency from resonance, decay rates of atomic level populations, Rabi frequency of the control field, and the density of doped nanocrystals.

The changes in the refractive index n and the propagation constant of the probe signal k are described by

$$\delta n = n\frac{\chi'}{2}, \qquad (23)$$

$$\delta k = 2\pi\frac{\nu\delta n}{c}, \qquad (24)$$

where ν and c are the frequency and velocity of light in vacuum, respectively. By using $\delta\phi = \delta k L/2$, we obtain the required phase shift for reading the stored data (L is the perimeter of the ring resonator).

3. Simulation results

By using of Y-type four level and Λ-type three level quantum dots with appropriate parameters, we obtained the required gain and phase difference at a wavelength of 1.55 μm. For Y-type four level quantum dots, the wavelength dependences

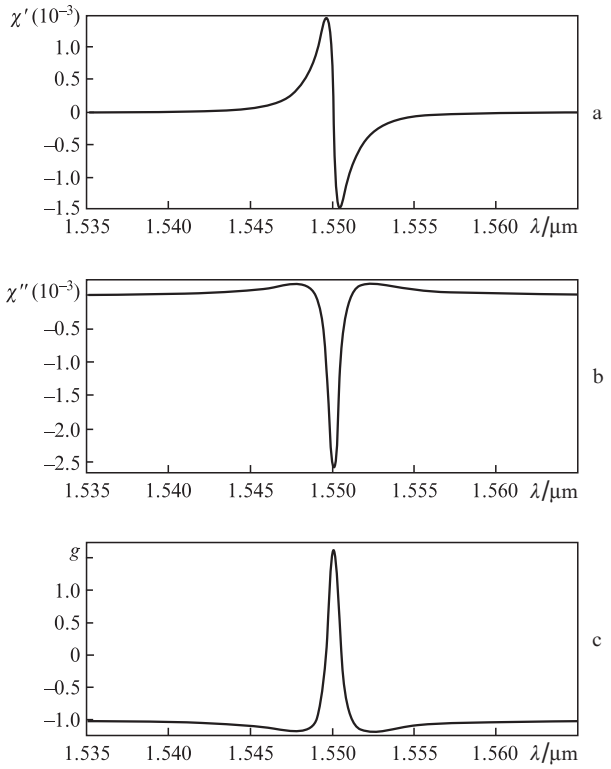

Figure 3. Wavelength dependences of (a) real and (b) imaginary parts of the susceptibility and of (c) the gain in the Y-type four level quantum dots at $\gamma_1 = 10^6$ s^{-1}, $\gamma_2 = \gamma_3 = 2\times10^{10}$ s^{-1}, $N_a = 7.07\times10^{21}$ cm^{-3}, $\wp_{ab} = 8.01\times10^{-29}$ C m, $E_p = 1.3166$ V m^{-1}, $E_{c1} = 2.0143\times10^5$ V m^{-1}, $E_{c2} = 1.988\times10^5$ V m^{-1}, $\Delta_2 = -\Delta_1$, $\Delta_3 = 0$, $\phi_1 = \phi_2 = \phi_3 = 0$.

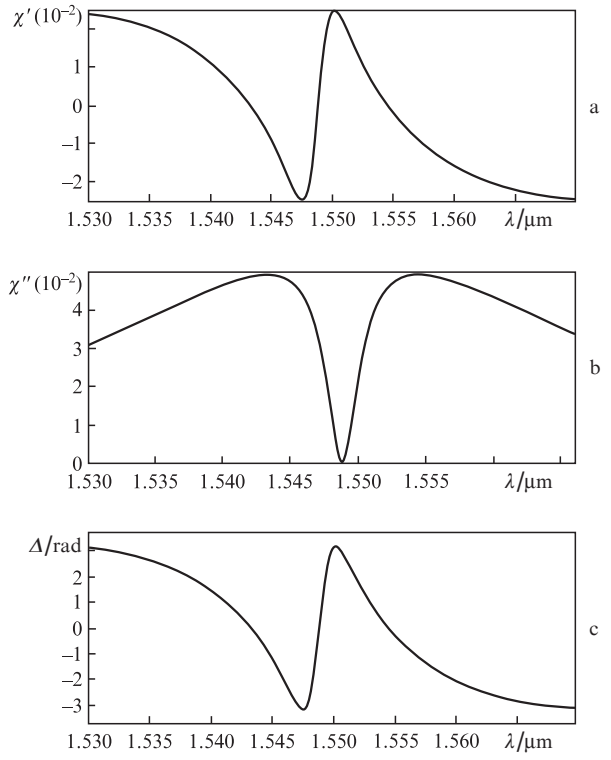

Figure 4. Wavelength dependences of (a) real and (b) imaginary parts of the susceptibility and of (c) the phase shift in the Λ-type three level quantum dots at $\gamma_1 = 1\times10^{12}$ s^{-1}, $\gamma_2 = \gamma_3 = 1\times10^8$ s^{-1}, $N_a = 9\times10^{21}$ cm^{-3}, $\wp_{ab} = 8.01\times10^{-29}$ C m, $E_{c1} = 6.5828\times10^5$ V m^{-1}.

of the real and imaginary parts of susceptibility and gain are shown in Fig. 3.

For Λ-type three level quantum dots, the spectral dependences of the real and imaginary parts of susceptibility and the phase shift are illustrated in Fig. 4. One can see that the phase required to read the stored data is equal to π and achieved at $\lambda = 1.55$ μm.

In simulating the cell operation in time, we used an InP ring of length $L = 2\pi r \approx 126$ μm and assumed that the required gain is ensured by InGaAsP quantum dots as the gain medium. In this case, the typical effective refractive index is $n_{\text{eff}} = 2.8$ and the loss is, as a rule, from 15 to 40 cm^{-1} (α = 25 cm^{-1} [11]).

Figure 5 shows the temporal parameters of the all-optical memory cell. When the data bit is injected into the memory cell, the data is stored during 33.19 ps (Fig. 5c). One can see that whenever there appears the required phase shift after applying the control field to the phase shifter segment, we can read the stored data.

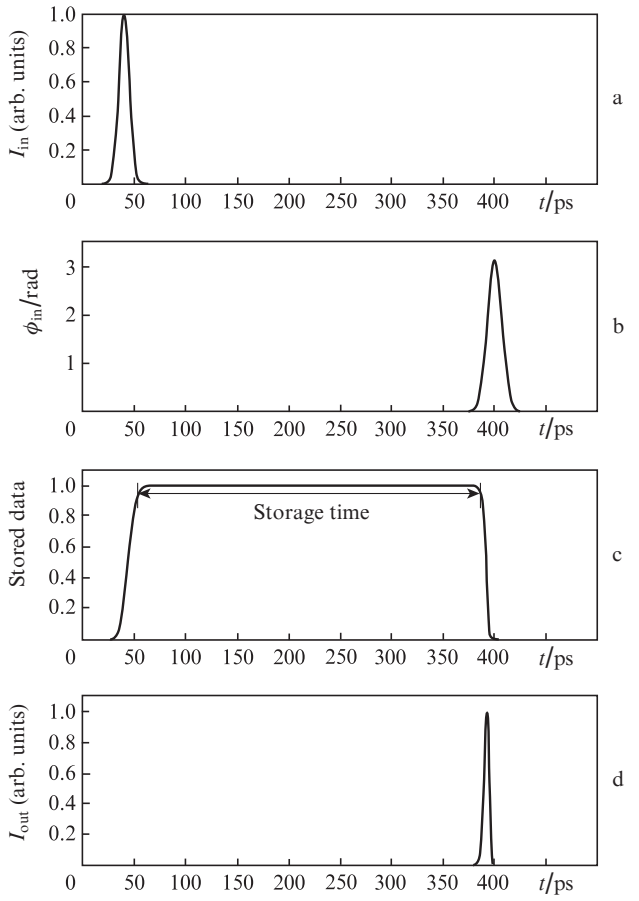

Figure 5. Temporal characteristics of the memory cell. (a) The input pulse with the FWHM $\tau_{1/2} \approx 11.75$ ps, (b) the phase-shifter pulse with the FWHM $\tau_{1/2} \approx 16.6$ ps, (c) the pulse of the data stored in the micro-ring resonator, (d) and the pulse of the read-out information with the FWHM $\tau_{1/2} \approx 5.7$ ps.

4. Conclusions

We have designed a loadable and erasable all-optical memory cell due to LWI and EIT effects. To compensate for the fibre loss, we have used LWI. Then, to read out stored data from the memory cell, we have produced an additional phase in the upper ring due to EIT. Also, we have illustrated that the time required to read the stored data can be reduced to 5.7 ps. This structure has more advantages over other structures, because it is miniaturised for further integration and does not need an additional optical filter for high speed operation. Besides, the rate of the designed memory cell is higher than that in the previously reported approaches. We have also analysed the frequency response of the proposed device.

References

1. Rabiei P., Steier W.H. *IEEE*, **2**, 517 (2001).
2. Chu S.T., Little B.E., Pan W., Kaneko T., Kokubun Y. *IEEE Photon. Technol. Lett*., **11**, 1426 (1999).
3. Little B.E., Chu S.T., Absil P.P., Hryniewicz J.V., Johnson F.G., Seiferth F., Gill D., Van V., King O., Trakalo M. *IEEE Photon. Technol. Lett*., **16**, 2263 (2004).
4. Popovic M.A., Barwicz T., Watts M.R., Rakich P.T., Socci L., Ippen E.P., Kartner F.X., Smith H.I. *Opt. Lett*., **31**, 2571 (2006).
5. Almeida V.R., Barrios C.A., Panepucci R.R., Lipson M. *Nature*, **431**, 1081 (2004).
6. Xu Q., Schmidt B., Pradhan S., Lipson M. *Nature*, **435**, 325 (2005).
7. Chao C.Y., Guo L.J. *Appl. Phys. Lett*., **83**, 1527 (2003).
8. Hill M.T., Dorren H.J.S., De Vries T., Leijtens X.J.M., Den Besten J.H., Smalbrugge B., Oel Y.S., Binsma H., Khoe G.D., Smit M.K. *Nature*, **432**, 206 (2004).
9. Johnson N.C., Harrison J.A., Blow K.J. *Opt. Commun*., **281**, 4464 (2008).
10. Poustie A.J., Kelly A.E., Manning R.J., Blow K.J. *Opt. Commun.*, **154**, 277 (1998).
11. Ding Y., Zhang X.A., Zhang X.N., Huang D. *Opt. Commun*., **281**, 5315 (2008).
12. Ding Y., Zhang X.A., Zhang X.N., Huang D. *Opt. Express*, **17**, 12835 (2009).
13. Ngo N.Q. *Appl. Opt*., **45**, 6785 (2006).
14. Liying Z., Zhengdong L., Jun C. *Mechanics & Astronomy*, **48**, 593 (2005).